IEEE Access
Multidisciplinary | Rapid Review | Open Access Journal

Received February 13, 2017, accepted April 24, 2017, date of publication May 4, 2017, date of current version July 7, 2017.

Digital Object Identifier 10.1109/ACCESS.2017.2700994

Phase-Coded Stepped Frequency Linear Frequency Modulated Waveform Synthesis Technique for Low Altitude Ultra-Wideband Synthetic Aperture Radar

MING YAM CHUA[1,2], (Member, IEEE), VOON CHET KOO[2], (Senior Member, IEEE), HENG SIONG LIM[2], (Senior Member, IEEE), AND JOSAPHAT TETUKO SRI SUMANTYO[1], (Senior Member, IEEE)

[1]Center for Environmental Remote Sensing, Chiba University, Chiba 263-8522, Japan
[2]Faculty of Engineering and Technology, Multimedia University, Melaka 75450, Malaysia

Corresponding author: Ming Yam Chua (e-mail: mychua@chiba-u.jp)

This work was supported in part by the Minister of Higher Education Malaysia under Grant 203.PJJAUH.6711279 and in part by the Japan International Cooperation Agency.

ABSTRACT This paper discusses a new waveform synthesis technique particularly suitable for low altitude ultra-wideband (UWB) synthetic aperture radar (SAR) systems. The proposed technique synthesizes a phase-coded UWB chirp by transmitting a burst of coherent phase-coded sub-band chirp pulses and combining the collected echoes using a special digital signal processing (DSP) algorithm. A lab prototype is built for the feasibility study and validation of the proposed technique. From the results, it is clearly shown that 1) the proposed technique can synthesize UWB chirp pulses; 2) the proposed DSP algorithm can combine the collected sub-band echoes into an echo of a wider bandwidth; and 3) the proposed technique can improve the range resolution of the SAR system without altering much of its system design. The main advantage of the proposed technique is that it can improve the range resolution of an existing SAR system without the need to increase the baseband bandwidth of the system.

INDEX TERMS Chirp modulation, field programmable gate arrays, radar equipment, synthetic aperture radar, ultra-wideband radar.

I. INTRODUCTION

Synthetic Aperture Radar is a popular multi-purpose active sensor that is capable for all-weather and day-to-night missions. SAR is a modern tool that employs the pulse compression technique to improve the resolution of its system whilst maintaining the pulse width of its transmitting signal [1], [2]. In SAR, the matched filtering technique is used to compress a conventionally wide pulse chirp into a very narrow impulse response.

The range resolution of a SAR system is inversely proportional to the bandwidth of its transmitting signal. A wider bandwidth SAR sensor has the better capability in distinguishing targets that are located near each other. The SAR system has stringent requirement in the Time Bandwidth Product (TBP) of its signal. The TBP determines the Pulse Compression Ratio (PCR), which is the quantitative measure of the range resolution improvement factor of the SAR system, as compared to an un-modulated pulse radar.

A large bandwidth chirp signal (up to a few Gigahertz in the K-band) is synthesized using a Voltage Controlled Oscillator (VCO). However, the sweep rate of the VCO is low (in milli-seconds) and thus, is not suitable for use in a pulsed SAR system [3]. Apart from this, a high TBP chirp signal (for example, with bandwidth of 250 MHz and pulse width of $<10\ \mu$s) can be easily synthesized by digital approach using a Digital to Analog Converter (DAC), but the synthesizable bandwidth is limited to the sampling speed of the DAC. Furthermore, increasing the sampling speed of the DAC will increase the requirement of the Analogue-to-Digital Converter (ADC) sampling speed.

In the past few decades, it has been the goal of radar system researchers to propose SAR waveform synthesis

techniques that could synthesize bandwidths as wide as possible using existing state of the art technology [4]–[9]. In this paper, a new UWB SAR waveform synthesis technique using a hybrid of analogue and digital approach is proposed, namely the Phase Coded Stepped Frequency Linear Frequency Modulated (PC-SF$_c$-LFM). The detailed explanation of the technique is discussed in Section II and Section III. Section IV-A describes the development work of a Field Programmable Gate Array (FPGA) based baseband waveform synthesizer while Section IV-B describes the experimental setup for validation of the proposed technique. Finally, the experimental results and the discussion of the findings are presented in Section V.

II. SF$_c$-LFM WAVEFORM SYNTHESIS TECHNIQUE

Traditionally, a SAR transmits a single burst of LFM modulated pulse at every Pulse Repetition Interval (PRI) [10]. Mathematically, the baseband LFM pulse is formulated as,

$$x_b(t) = A \cdot \prod\left(\frac{t}{T_p}\right) \cdot e^{j\pi(\alpha t^2 - Bt)} \tag{1}$$

where A is the peak-to-peak amplitude, α is the chirp rate, T_p is the chirp pulse width, and B is the bandwidth of the baseband LFM signal. For a heterodyne SAR system, employing the up-conversion methodology, the baseband LFM signal is up-converted to RF carrier frequency band, f_c, [11]–[13] and can be described using the equation below,

$$x_t(t) = A \cdot \prod\left(\frac{t}{T_p}\right) \cdot e^{j\pi(\alpha t^2 - Bt)} \cdot e^{j2\pi f_c t} \tag{2}$$

In SF$_c$-LFM, instead of a single burst, multiple bursts of identical LFM pulse are transmitted at every PRI interval. Within a PRI, each pulse is separated by an intra-PRI interval, t_{pri_int}. The main reason to include a pulse-to-pulse separation is to retain the radar system range ambiguity by ensuring the current listening echo does not overlap with the transmission of the succeeding pulse. The baseband intra-pulses within a PRI for SF$_c$-LFM can be formulated as the equation below,

$$x_n(t_m) = A \cdot \sum_{n=1}^{N} \prod\left(\frac{t}{T_p}\right) \cdot e^{j\pi(\alpha t^2 - Bt)} \tag{3}$$

where,

N = number of transmitted pulses within an PRI interval
n = integer number of 1, 2, 3, , N
t_m = $t - (n-1)t_{pri\_int}$
t_{pri_int} = intra-PRI interval

An example of a time-frequency plot of four-burst ($N = 4$) SF$_c$-LFM baseband LFM pulse with four bursts of identical pulse is depicted in Figure 1. Figure 2 is the plot for an example baseband SF$_c$-LFM pulse in time.

In SF$_c$-LFM, each pulse is mixed with different adjacent carrier frequencies. For design simplicity, an assumption is made where only even number of intra-pulses are transmitted (N is an even number and $N \geq 2$). Equation (3) then becomes,

$$x_{n\_rf}(t_m) = A \cdot \sum_{n=1}^{N} \prod\left(\frac{t}{T_p}\right) \cdot e^{j\pi(\alpha t_m^2 - Bt_m)} \cdot e^{j2\pi f_n t_m} \tag{4}$$

where f_n is the desired adjacent carrier frequency denoted as,

$$f_n = f_c + \left[(n-1) - \frac{N}{2} + 0.5\right]B \tag{5}$$

Theoretically, the effective bandwidth B_{eff}, and effective pulse duration, T_{eff}, of SF$_c$-LFM are as simple as multiplying the bandwidth, B, and the pulse duration, T_p, of the baseband LFM pulse with the total number of intra-pulses transmitted, N. The range resolution of a SAR system that employs SF$_c$-LFM scheme signal then will be improved for N times. In summary,

$$B_{eff} = N \times B \tag{6}$$

$$T_{eff} = T \times T_p \tag{7}$$

$$\Delta R_{eff} = \frac{c}{2B_{eff}} \tag{8}$$

Figure 3 illustrates the up-conversion process of the baseband intra-pulses into its respective adjacent carrier frequency which yields in widening its effective pulse duration

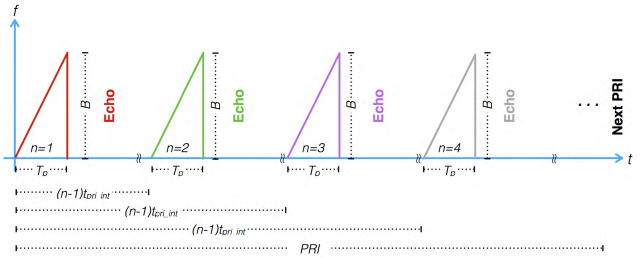

FIGURE 1. Time-frequency plot for SF$_c$-LFM ($N = 4$).

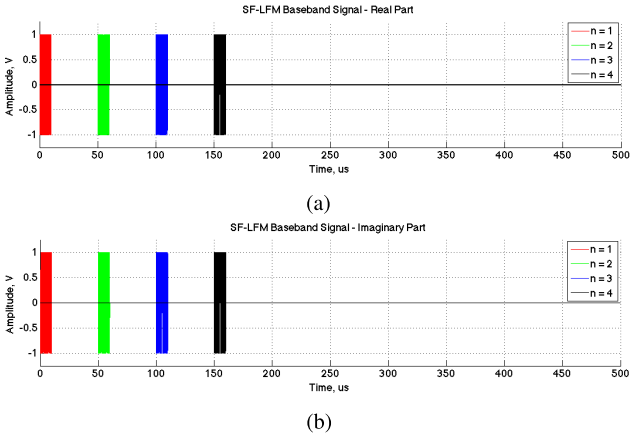

FIGURE 2. Time domain plot of SF$_c$-LFM baseband signal ($N = 4$, $B = 80$ MHz, $T_p = 10\mu$s, $t_{pri_int} = 50\mu$s). (a) In-phase component. (b) Quadrature component.

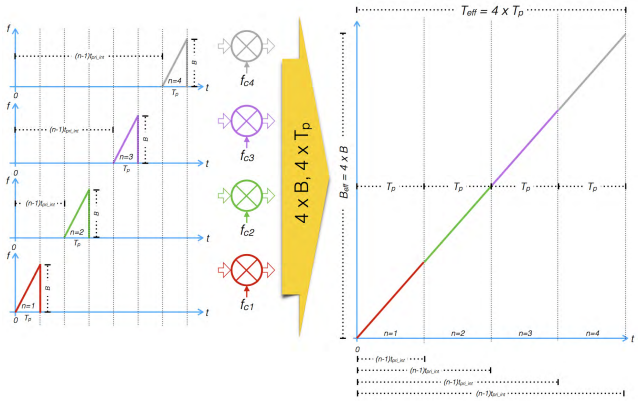

FIGURE 3. Proposed SF_c-LFM modulation scheme.

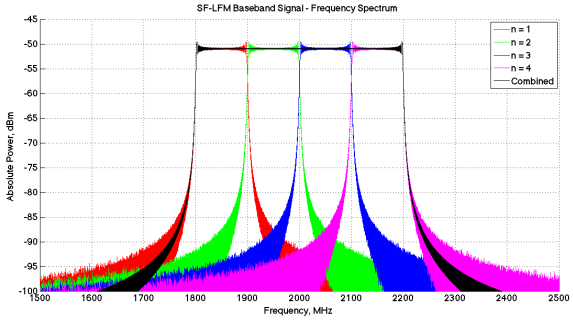

FIGURE 4. Simulated SF_c-LFM waveform frequency spectrum.

and bandwidth. An example of SF_c-LFM simulated waveform spectrum is shown in Figure 4.

The intra-pulses in the carrier band are transmitted as in a regular SAR system. Each intra-pulse echo is then mixed with its own respective carrier signal, so that it is down-converted to baseband and digitized. At each intra-pulse interval, t_{pri_int}, a trigger signal is sent to the SAR processor so as to initiate the data recording. Thus, the SF_c-LFM SAR system records N times more echoes as compared to a regular SAR system. It shall be noted that the initial time for each recorded echo frame is at $t - (n-1)\,tpri\_int$.

The collected intra-pulses are stored as a 2-dimensional array of digital data with N pulses recorded for every PRI. Before the recorded data can be used for SAR image formation, it requires an additional Digital Signal Processing (DSP) algorithm to reconstruct all recorded intra-pulses into its single pulse equivalent, from which the single pulse equivalent is to be,

$$x_{equi}(t) = A \cdot \prod\left(\frac{t}{T_{eff}}\right) \cdot e^{j\pi\left(\alpha_{eff}t^2 - B_{eff}t\right)} \tag{9}$$

where,

B_{eff} = Effective bandwidth
T_{eff} = Effective pulse width
α_{eff} = Effective LFM rate = $B_{eff} \times T_{eff}$

Figure 5 illustrates the time-frequency plot of the signal reconstruction process for a record of 4 intra-pulses ($N = 4$)

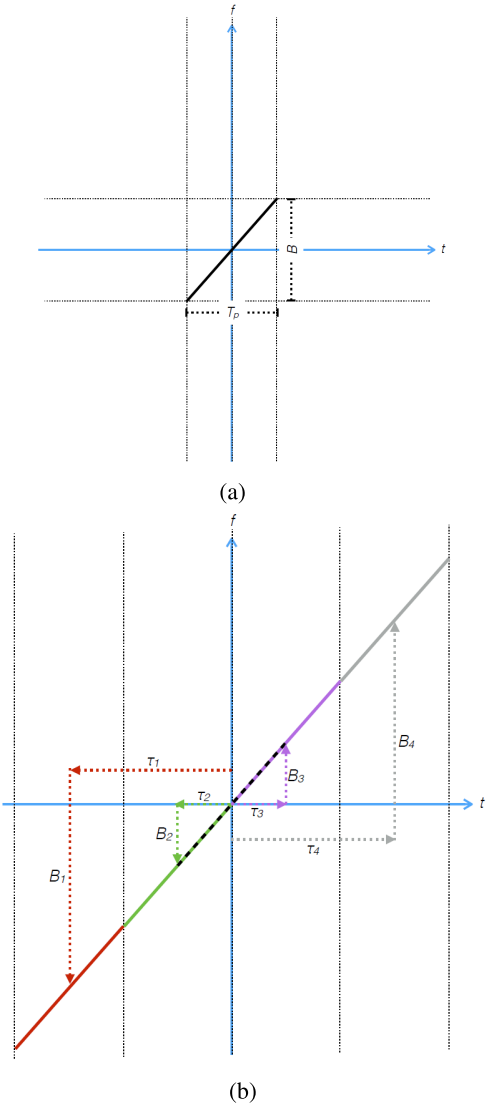

FIGURE 5. SF_c-LFM pulse reconstruction algorithm ($N = 4$). (a) Collected intra-pulses echoes. (b) Signal reconstruction algorithm.

SF_c-LFM waveform. The received echo for each of the intra-pulses can be formulated as,

$$x_n(t_n) = A \cdot \prod\left(\frac{t_n}{T_p}\right) \cdot e^{j\pi\left(\alpha t_n^2 - Bt_n\right)} \cdot e^{j2\pi f_c t_n} \tag{10}$$

All recorded echoes will reside at the origin on the time-frequency plot of the waveforms, as shown in the Figure 5(a). In the signal reconstruction process, the collected echoes will be re-arranged into their respective frequency bands and time slots. The signal reconstruction process can be summarized as adding a time shift of, τ_n, a phase shift of, B_n, into the respective echo pulses. Hence, (10) becomes,

$$x_n(t_n - \tau_n) = A_n \cdot \prod\left(\frac{t_n - \tau_n}{T_p}\right) \cdot e^{j\pi\left(\alpha(t_n - \tau n)^2 - B(t_n - \tau_n)\right)} \cdot e^{j2\pi f_c(t_n - \tau_n)} \cdot e^{j2\pi B_n(t_n - \tau_n)} \tag{11}$$

where,

$$\tau_n = \left[\left((n-1) - \frac{N}{2}\right) + 0.5\right] T_p \tag{12}$$

$$B_n = \left[\left((n-1) - \frac{N}{2}\right) + 0.5\right] B \tag{13}$$

Expanding (11),

$$x_{(t_n-\tau_n)} = A \cdot \prod \left(\frac{t_n - \tau_n}{T_p}\right) \cdot e^{\phi_r(t)} \tag{14}$$

where,

$$\phi_r(t) = j\pi \left(\alpha \left(t_n - \tau_n\right)^2 - B\left(t_n - \tau_n\right)\right) + j2\pi f_c \left(t_n - \tau_n\right) + j2\pi B_n \left(t_n - \tau_n\right) \tag{15}$$

Expanding (15), yields,

$$\phi_r(t) = j\pi \left[\alpha t^2 - 2\alpha t\tau_n - Bt + 2f_c t + 2B_n t + \alpha\tau_n^2 + B\tau_n - 2f_c\tau_n - 2B_n\tau_n\right] \tag{16}$$

Down-converting (14) into baseband, the baseband phase of the received signal ϕ_{r_b}, is,

$$\phi_{r\_b}(t) = j\pi \left[\alpha t^2 - 2\alpha t\tau_n - Bt + 2B_n t + \alpha\tau_n^2 + B\tau_n - 2f_c\tau_n - 2B_n\tau_n\right] \tag{17}$$

Re-arranging (17),

$$\phi_{r\_b}(t) = j\pi \left[\left(\alpha t_n^2 - Bt_n\right) - 2\alpha t_n\tau_n + 2B_n t_n + \alpha\tau_n^2 + B\tau_n - 2f_c\tau_n - 2B_n\tau_n\right] \tag{18}$$

From the equation, it is shown that the phase of each collected echo intra-pulse should be shifted with ϕ_n, where ϕ_n can be quantified as,

$$\phi_n = j\pi(-2\alpha t_n\tau_n + 2B_n t_n + \alpha t_n^2 + B\tau_n - 2f_c\tau_n - 2B_n\tau_n) \tag{19}$$

In order to verify the functionality of the proposed technique, simulated intra-pulses are generated using Matlab®. The intra-pulses are re-constructed into their equivalent pulses using the algorithm as described above. Figure 6 and Figure 7 show the generated single target intra-pulses, reconstructed pulses and the ACF of the reconstructed pulses for $N = 4$. Figure 8 and Figure 9 show the generated multiple targets intra-pulses, reconstructed pulses and the ACF of the reconstructed pulses for $N = 4$. The simulation results clearly showed that the proposed signal reconstruction algorithm is able combine the intra-pulses into a wider bandwidth and pulse width signal.

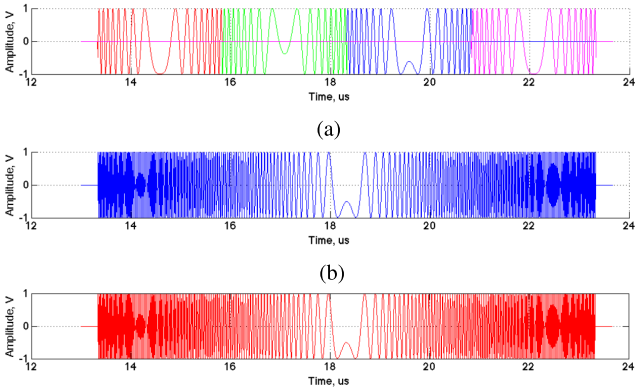

FIGURE 6. Simulated sub-pulses with single point target ($N = 4$). (a) Baseband intra-pulses. (b) Reference pulse. (c) Reconstructed pulse.

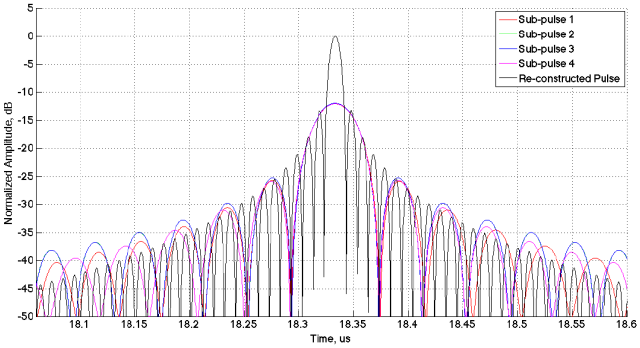

FIGURE 7. ACF of reconstructed baseband pulse (simulated).

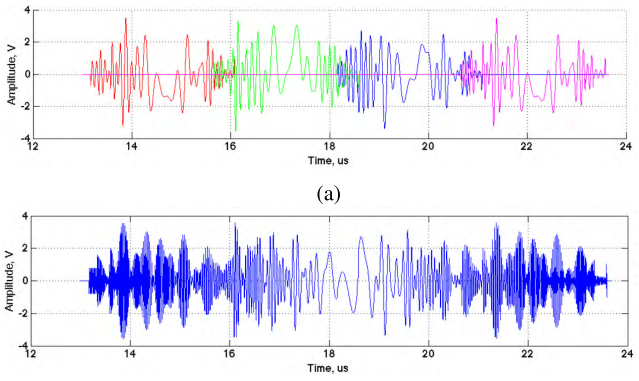

FIGURE 8. Simulated sub-pulses of four point targets ($N = 4$). (a) Baseband intra-pulses. (b) Reconstructed pulse.

III. PHASE CODED SF$_c$-LFM

SF$_c$-LFM is able to improve the waveform bandwidth and pulse width by transmitting N intra-pulses at every PRI interval. The echo of the intra-pulses is down-converted and recorded by a data acquisition system. These recorded intra-pulses are then combined into an equivalent large bandwidth and wide pulse width signal as in a conventional SAR system.

In SAR signal processing, the baseband waveform parameters such as bandwidth and pulse width are needed for

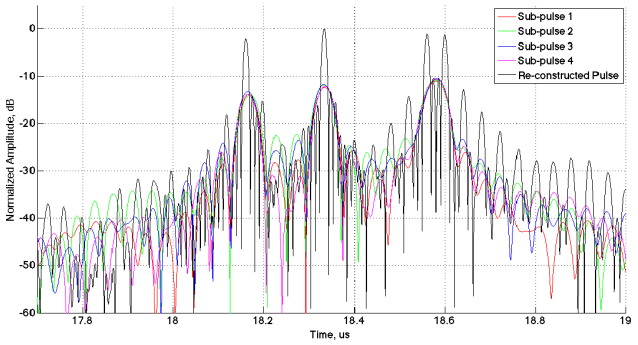

FIGURE 9. ACF of reconstructed baseband pulse (simulated).

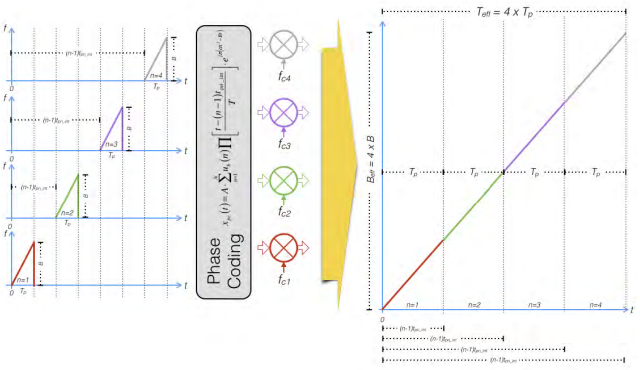

FIGURE 10. Proposed phase coded SF_c-LFM modulation scheme.

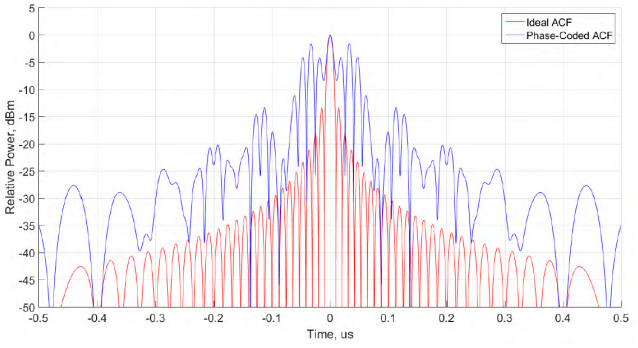

FIGURE 11. ACF of BPSK-coded SF_c-LFM pulse (K = 8).

reference signal generation in SAR image formation. In order to enhance the security level of an SF_c-LFM SAR system, the intra-pulses are encrypted with different orthogonal phase during the baseband waveform generation. Before the recorded echo pulses are combined into its equivalent LFM pulse, these intra-pulses have to be decrypted by removing the additional phase introduced during its signal generation. This additional phase coding scheme allows signal protection mechanism to be embedded into the SF_c-LFM SAR system where the receiver has to know the appropriate decoding scheme to recover the SAR image. In phase coded SF_c-LFM, the intra-pulses are modulated with different phase coding

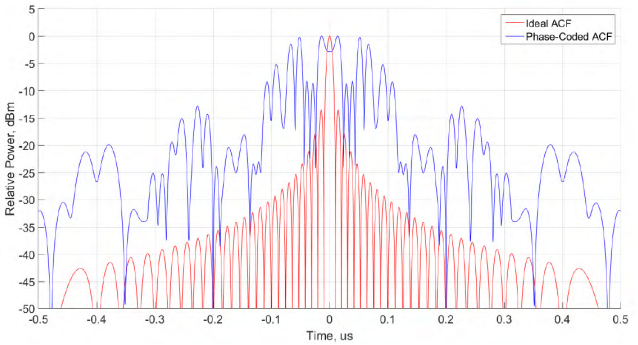

FIGURE 12. ACF of BPSK-coded SF_c-LFM pulse (K = 16).

scheme given by,

$$x_{pc}(t) = A \cdot \sum_{n=1}^{K} u_b(n) \cdot \prod \left[\frac{t - (n-1)t_{pri\_int}}{T} \right] \cdot e^{j\pi(\alpha t^2 - Bt)} \tag{20}$$

where $u_b(n)$ is the implemented phase coding scheme.

Figure 10 illustrates the proposed phase coded SF_c-LFM SAR waveform synthesis technique. The SF_c-LFM waveform synthesis technique remains the same as illustrated in Section II. An additional phase coding process is introduced on the intra-pulses before the pulses are up-converted into its respective frequency band. The phase coding process is performed by altering the phase control register (PHA) for each intra-pulse during the signal generation process. The detailed discussion on the real-time reconfigurable Field Programmable Gate Array (FPGA) based Direct Digital Synthesis (DDS) chirp generator system can be found in [14] and [15]. During the signal re-construction process, the phase decoding will be carried out and it is an inverse process of phase coding.

For illustration purposes, Binary Phase Shift Keying (BPSK) and Quadrature Phase Shift Keying (QPSK) phase coding scheme are implemented. In BPSK,

$$u_b(n) = e^{j\pi(1-b)} \tag{21}$$

where $b = 0, 1$. The BPSK coding scheme yields to two phases, 0 and π, for binary keyword "0"and "1", respectively.

The phase-coded intra-pulses are combined into its single burst equivalent and their ACF plots are plotted in Figure 11 and Figure 12 for $K = 8$ and $K = 16$ respectively.

The BPSK scheme requires phase changes of π on the pulse-to-pulse relative phase in phase coded SF_c-LFM. In QPSK, the phase change is, $\pi/4$, thus,

$$u_b(n) = e^{j\pi(2b+1)\frac{\pi}{4}} \tag{22}$$

where $b = 0,1,2,3$ for binary phase code "00", "01", "10", and "11"respectively. Thus, the QPSK coding schemes generates four orthogonal phases, with angles of $\pi/4$, $3\pi/4$, $5\pi/4$, and $7\pi/4$.

The ACF plots for QPSK-coded SF_c-LFM modulation scheme are shown in Figure 13 and Figure 14 for $K = 8$

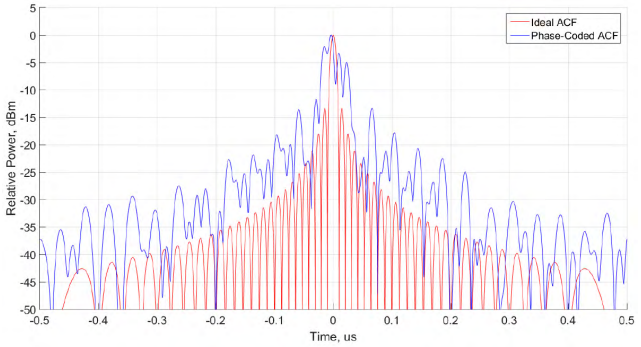

FIGURE 13. ACF of QPSK-coded SF_c-LFM pulse (K = 8).

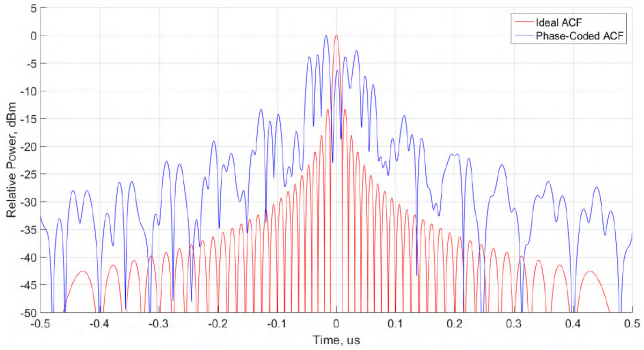

FIGURE 14. ACF of QPSK-coded SF_c-LFM pulse (K = 16).

TABLE 1. Custom designed altera cyclone IV FPGA board for SF_c-LFM.

Module	Specifications
FPGA	• Altera EP4CE22E22C7N • 22,320 LEs • 594 Kbits total memory • 66 18×18-bit multipliers • 4 General Purpose PLLs • 153 user I/Os
Peripherals	• USB to UART interface • 4 ways user DIP switch • 3×8 ways I/O • 1 way user push button • 4 ways user LED indicator
Digital-to-Analog Converter	• 210 MSPS maximum sampling rate • 2 channels • 14-bits data resolution

and $K = 16$ respectively. From the ACF for BPSK and QPSK coded SF_c-LFM waveform, it is shown that without proper phase decoding in SF_c-LFM waveform, the formed SAR image will not be focused.

IV. HARDWARE IMPLEMENTATION OF SF_c-LFM SCHEME ON FPGA BOARD

In order to verify the functionality of the proposed SF_c-LFM SAR signal synthesis technique, a lab experimental setup is constructed. The discussion of the setup is covered in two sub-sections; namely, an FPGA-based real-time reconfigurable phase coded SF_c-LFM SAR signal synthesizer and an SF_c-LFM RF transmitter.

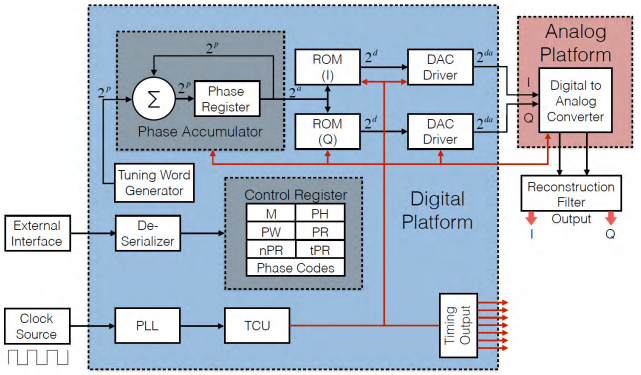

FIGURE 15. Block diagram of the proposed phase coded SF_c-LFM baseband waveform synthesizer.

TABLE 2. SF_c-LFM waveform design parameters.

Module	Parameter	Value
Clock	External reference clock	10 MHz
	Internal reference clock	200 MHz
UART	Baud rate	115200 baud
	Format	1 start, 8 data
		1 stop, no parity
Phase Accumulator	Phase wheel width	24 bits
	Tuning word width	15 bits
LUT (Each I & Q)	Table size	32768 entries
	Data width	16 bits
TCU	Timing precision	5 ns
HS-DAC	Number of channel	2 channels
	Data width	200 MSPS
		(210 MSPS max)
	Data width	14 bits

A. FPGA-BASED SF_c-LFM WAVEFORM SYNTHESIZER

In order to synthesize the required baseband SF_c-LFM waveform, an FPGA-based reconfigurable waveform synthesizer has been designed and developed. The development work is an extension work for [14] and [15] with added SF_c-LFM Waveform synthesis capability. Figure 15 depicts the architecture of the proposed SF_c-LFM waveform synthesizer. The waveform synthesizer design parameters are tabulated in Table 2. As a summary, the phase accumulator remains as the core of the waveform synthesizer with reconfigurable capability in real-time. The developed synthesizer is capable of synthesizing the proposed SF_c-LFM scheme waveform with intra-pulse phase coding capability through the control register *nPR*, *tPR* and *Phase Codes*. Control signals such as digitizers trigger signal and RF signal generator control signal will be generated from the synthesizer as well.

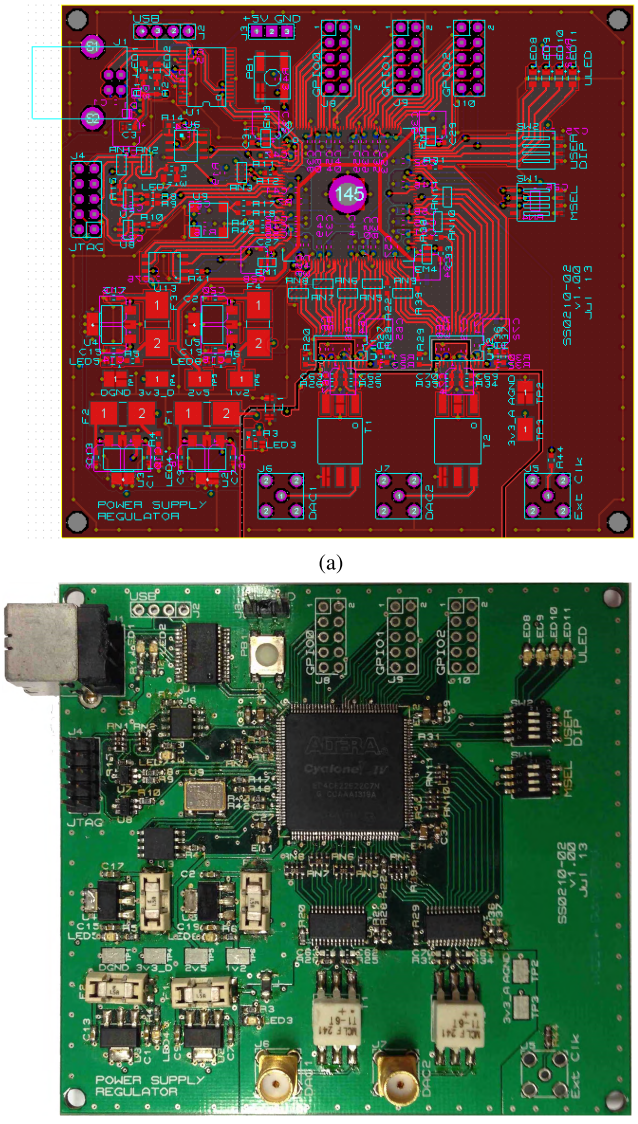

(a)

(b)

FIGURE 16. FPGA-based SF_c-LFM waveform synthesizer. (a) Printed circuit board layout design. (b) Assembled prototype.

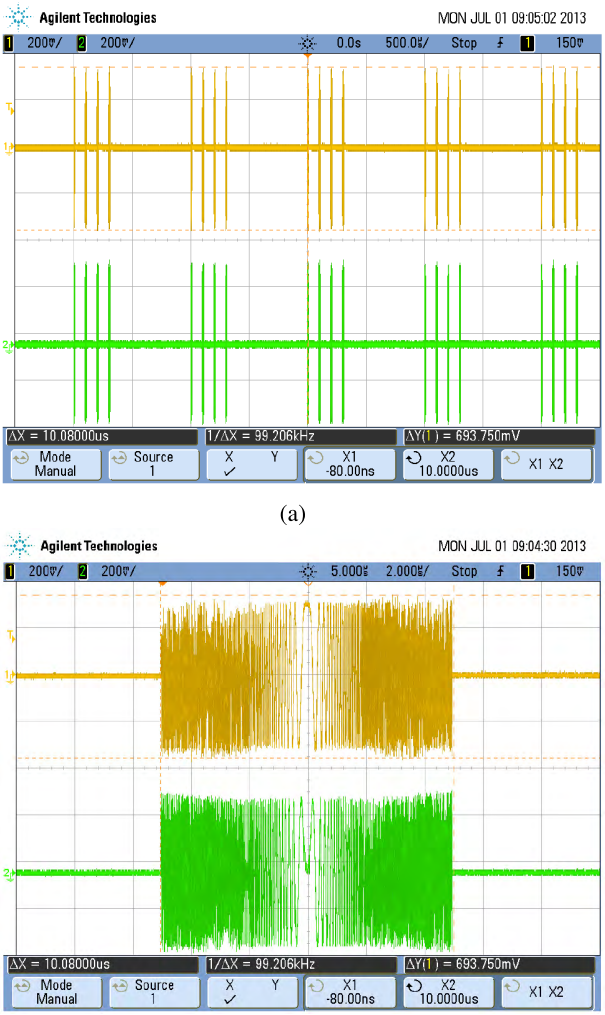

(a)

(b)

FIGURE 17. Phase coded SF_c-LFM baseband waveform ($N = 4$).

The proposed architecture is implemented on a custom-designed FPGA-based waveform synthesizer. Table 1 lists the major features of the custom-designed board. The board uses Altera Cyclone IV FPGA chips as its programmable core with on-board dual-channel, 14-bit, 420 MSPS Digital-to-Analogue Converter. The design layout and the assembled board are shown in Figure 16. The board employs 4-layer FR4 stack-up configuration and are designed with careful considerations in complying to High Speed Printed Circuit Board (HS-PCB) requirements. Besides DACs, the board has several on-board peripherals such as UART to TTL level converter, 4 User LEDs, 8-way User DIP Switch, and 8-way Parallel IO, which enable interfacing with external devices.

An example of SF_c-LFM baseband waveform generated using the FPGA-based waveform synthesizer is shown in Figure 17. Table 2 tabulates the SF_c-LFM waveform design parameters in hardware implementation.

B. SF_c-LFM RF TRANSMITTER EXPERIMENTAL SETUP

The baseband SF_c-LFM scheme signal has to be up-converted to its respective carrier band as described in (4) and (5). Figure 18 illustrates the block diagram of the setup. In the transmitter, the baseband intra-pulses are up-converted to its respective carrier using an off-the-shelf microwave quadrature modulator. An RF signal generator is used to generate the required stepped carrier signal for the up-conversion process. In order to ensure coherency in the transmitted intra-pulses, the selected signal generator should have low phase noise (<-120dBc/Hz @ 20 kHz offset) so that the noise contributed by phase difference between the intra-pulses will be insignificant. The up-converted intra-pulse is fed into a calibrated microwave delay line to simulate a single point target artificial microwave echo. The intra-pulses echoes are down-converted using an off-the-shelf microwave demodulator

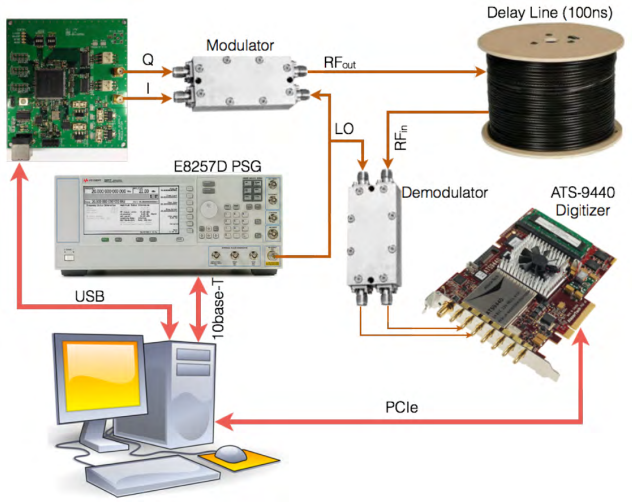

FIGURE 18. Block diagram of proof-of-concept experimental setup.

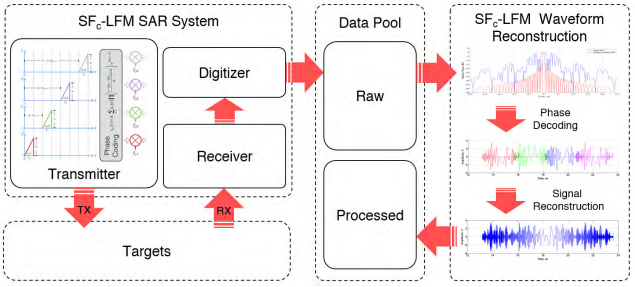

FIGURE 19. The process flow of the proof-of-concept experiment.

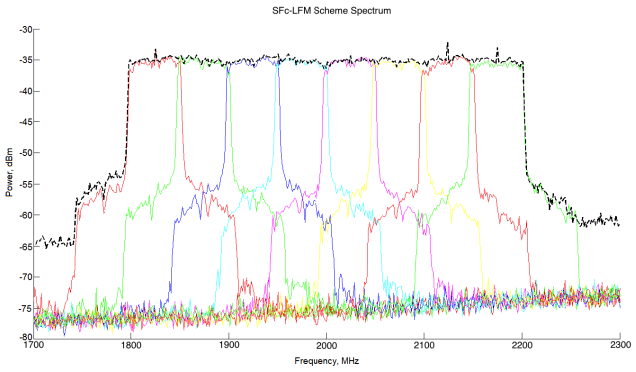

FIGURE 20. Frequency spectrum of SF_c-LFM ($N = 8$, $B = 50$ MHz): DSP combined spectrum (black colour), individual intra-pulse spectrum (other colours).

and recorded. Finally, the recorded data are further processed using the proposed DSP algorithm discussed in Sections II and III. Figure 19 illustrates the processes involved in the experiment.

Table 3 summarizes the SF_c-LFM signal parameters ($N = 8$). The intra-pulses are up-converted to different carrier frequencies, $f_1 - f_8$, as described in (5). Based on (6) and (7), for the generated SF_c-LFM signal, the effective bandwidth, B_{eff}, is 400 MHz and the effective pulse width, T_{eff}, is 80 μs.

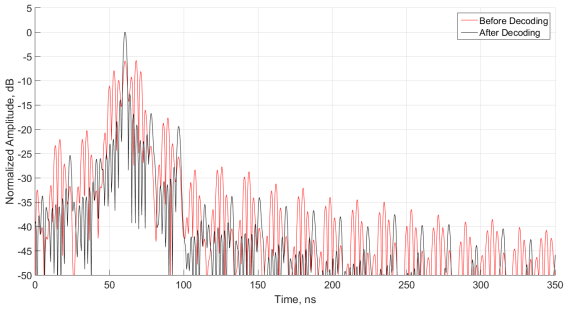

FIGURE 21. Match filter output comparison of SF_c-LFM received signal ($N = 8$) before and after phase decoding.

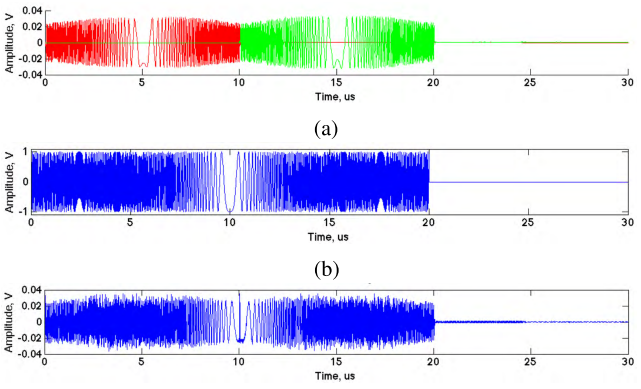

FIGURE 22. Recorded sub-pulses ($N = 2$, $t_d = 0$ ns). (a) Collected sub-pulses. (b) Reference signal. (c) Reconstructed baseband pulse.

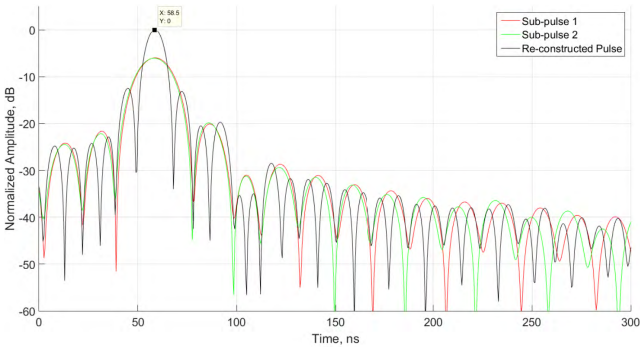

FIGURE 23. ACF of reconstructed baseband pulse ($N = 2$, $t_d = 0$ ns).

V. RESULTS AND FINDINGS

One of the advantages of the proposed SF_c-LFM waveform is the increase in its effective transmitted bandwidth, and hence dramatically enhances the range resolution of the SAR system in a cost effective way. With SF_c-LFM, a UWB SAR signal could be easily synthesized without much hardware alteration or upgrade on the existing SAR system.

By using the proposed SF_c-LFM scheme, SAR intra-pulses with nominal bandwidth are transmitted and the intra-pulses echoes are collected for signal re-construction. During the SF_c-LFM signal reconstruction process, the intra-pulses are combined into its equivalent large bandwidth and wide

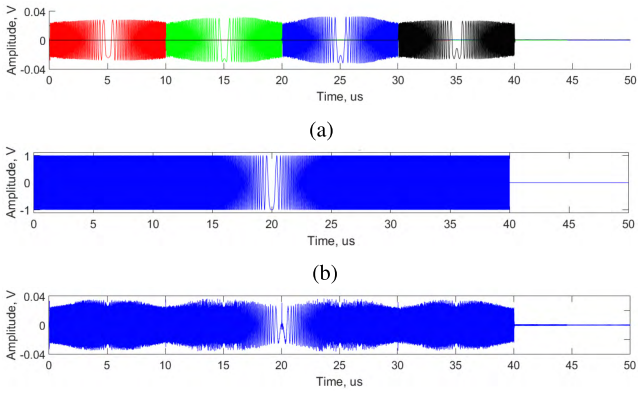

FIGURE 24. Recorded sub-pulses ($N = 4$, $t_d = 0$ ns). (a) Collected sub-pulses. (b) Reference signal. (c) Reconstructed baseband pulse.

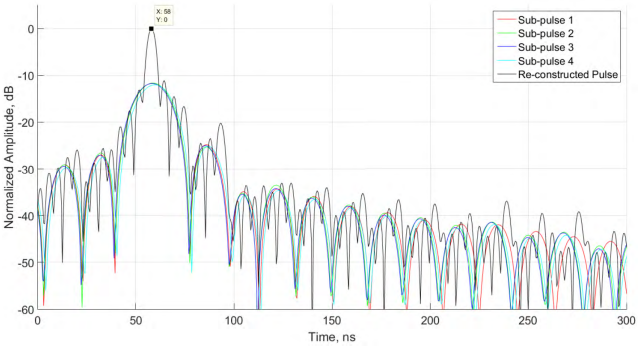

FIGURE 25. ACF of reconstructed baseband pulse ($N = 4$, $t_d = 0$ ns).

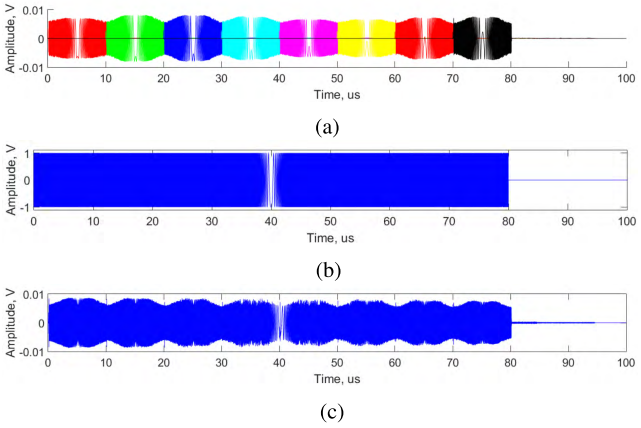

FIGURE 26. Recorded sub-pulses ($N = 8$, $t_d = 0$ ns). (a) Collected sub-pulses. (b) Reference signal. (c) Reconstructed baseband pulse.

pulse-width signal. The resultant signals are then processed to form a 2-dimensional SAR image.

From the frequency spectrum perspective, the transmitted intra-pulses occupy their respective frequency bands centered at different carrier frequencies as described in (4). The center frequency of each intra-pulse is described in (5). Figure 20 shows the frequency spectrum of each of the transmitted

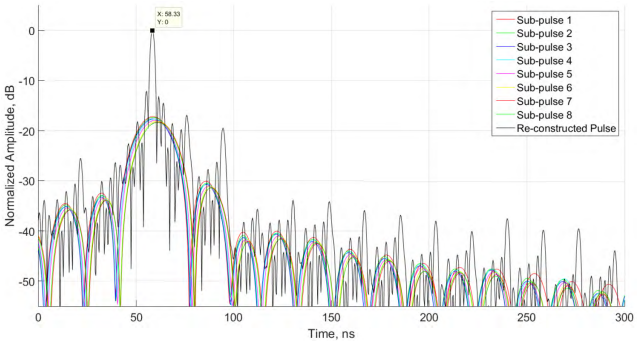

FIGURE 27. ACF of reconstructed baseband pulse ($N = 8$, $t_d = 0$ ns).

TABLE 3. SF_c-LFM waveform design parameters.

Parameters	Value
Number of intra-pulses, N	8
Intra-pulse bandwidth, BW	50 MHz
Pulse Repetition Frequency, PRF	1 kHz
Pulse Width, T_p	10 μs
Carrier Frequency, f_c	2000 MHz
• 1st carrier frequency, f_1	1825 MHz
• 2nd carrier frequency, f_2	1875 MHz
• 3rd carrier frequency, f_3	1925 MHz
• 4th carrier frequency, f_4	1975 MHz
• 5th carrier frequency, f_5	2025 MHz
• 6th carrier frequency, f_6	2075 MHz
• 7th carrier frequency, f_7	2125 MHz
• 8th carrier frequency, f_8	2175 MHz
Effective Bandwidth, B_{eff}	400 MHz
Effective Pulse Width, T_{eff}	80 μs

TABLE 4. Parameters for experimental setup.

Figure	Measurement Parameters
Figure 28 and Figure 29	t_d = 100 ns, N = 2
Figure 30 and Figure 31	t_d = 100 ns, N = 4
Figure 32 and Figure 33	t_d = 100 ns, N = 8
Figure 34 and Figure 35	t_d = 200 ns, N = 2
Figure 36 and Figure 37	t_d = 200 ns, N = 4
Figure 38 and Figure 39	t_d = 200 ns, N = 8

intra-pulse and the DSP combined spectrum of the resultant signal. It is observed that for 8 intra-pulse (N = 8) signals with each intra-pulse having 50 MHz baseband bandwidth, the combined spectrum shows a total of 400 MHz effective bandwidth (8 times improvement).

As discussed in Section II, the recorded echoes of SF_c-LFM are combined into an equivalent wide bandwidth signal in an additional signal re-construction process prior to the 2-D SAR image formation. The mathematical formulation of the signal reconstruction technique has been verified through a simulation using Matlab®.

Before the signal is reconstructed, a phase decoding process (or intra-pulses decryption) is required to remove the

TABLE 5. Peak side-lobe ratio (PSLR) comparison and improvement in impulse response width (IRW).

Number of intra-pulses N	Delay (ns)	Single-Pulse LFM PSLR(dB)	SF_c-LFM PSLR (dB)	Single-Pulse LFM PSLR (dB)	SF_c-LFM PSLR (dB)	Improvement (Estimated)	Improvement (Measured)
2	100	-13.36	-12.89	17.23	8.32	2.00	2.07
	200	-13.11	-12.92	17.23	8.33	2.00	2.07
4	100	-12.96	-12.02	16.70	4.03	4.00	4.14
	200	-12.85	-12.73	16.70	4.01	4.00	4.16
8	100	-12.92	-12.70	16.75	2.00	8.00	8.35
	200	-12.90	-11.25	16.75	1.98	8.00	8.43

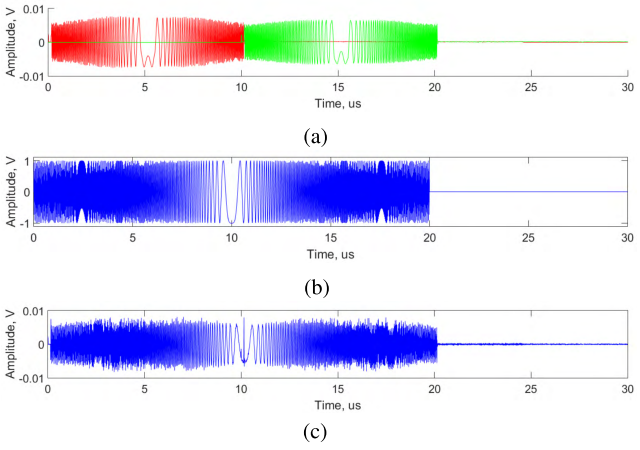

FIGURE 28. Recorded sub-pulses ($N = 2$, $t_d = 100$ ns). (a) Collected sub-pulses. (b) Reference signal. (c) Reconstructed baseband pulse.

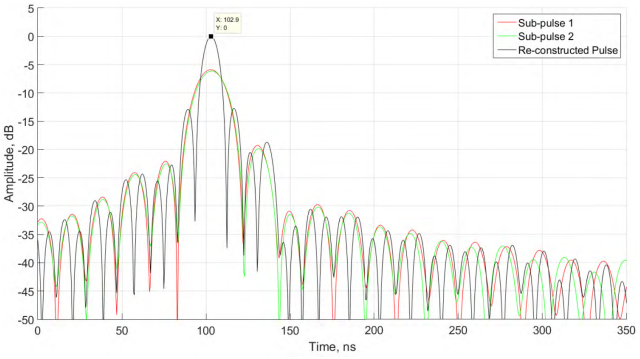

FIGURE 29. ACF of RECONSTRUCTED BASEBAND PULSE ($N = 2$, $t_d = 100$ ns).

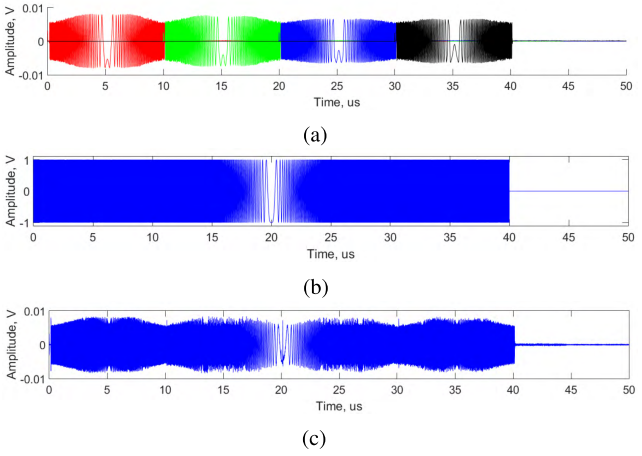

FIGURE 30. Recorded sub-pulses ($N = 4$, $t_d = 100$ ns). (a) Collected sub-pulses. (b) Reference signal. (c) Reconstructed baseband pulse.

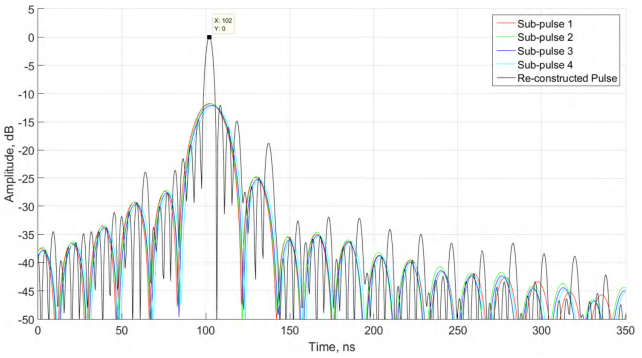

FIGURE 31. ACF of reconstructed baseband pulse ($N = 4$, $t_d = 100$ ns).

additional phase during the baseband SF_c-LFM signal generation. Figure 21 shows the comparison of matched filter output of the received SF_c-LFM signal, before and after phase decoding. It can be observed that the phase coded signal has been compressed into its equivalent impulse response after a proper decoding process.

In order to measure the internal delay contributed by the setup (microwave components, cables, connectors, FPGA board latency, etc.), the output of the transmitter is connected directly to the input of the receiver to emulate a delay, t_d, of 0 ns. Figure 22, Figure 24, and Figure 26 show the digitized echoes and the re-constructed signals of 2, 4, and 8 intra-pulses, respectively. From the matched filter output plot in Figure 23, Figure 25, and Figure 27, it is measured that the system internal delay is approximately 58.5 ns. The measured internal delay are deducted in subsequent measurements where an external delay line is connected to emulate a known microwave delay. The amplitude fluctuation observed in each of the sub-pulses is due to the uneven amplitude flatness in the microwave components.

Subsequently, the results of a subsequent measurement are presented. In the subsequent measurement, two

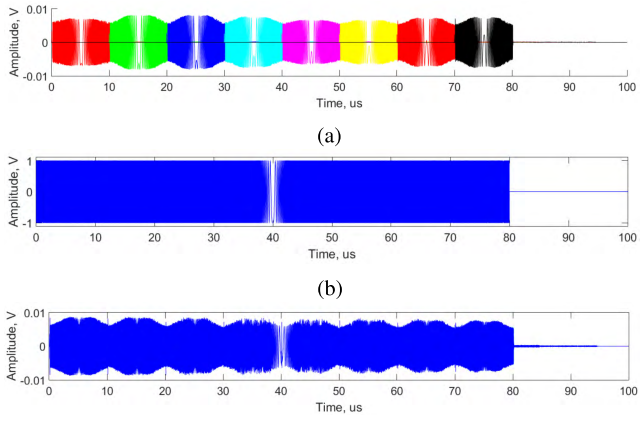

FIGURE 32. Recorded sub-pulses ($N = 8$, $t_d = 100$ ns). (a) Collected sub-pulses. (b) Reference signal. (c) Reconstructed baseband pulse.

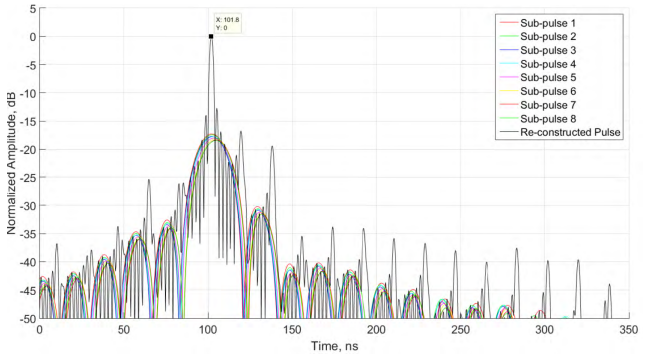

FIGURE 33. ACF of reconstructed baseband pulse ($N = 8$, $t_d = 100$ ns).

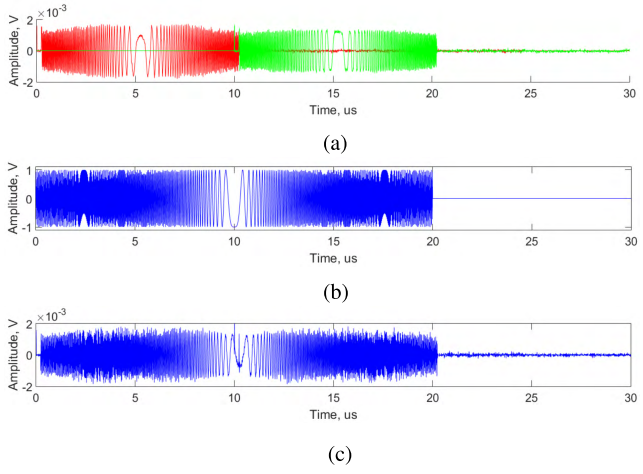

FIGURE 34. Recorded sub-pulses ($N = 2$, $t_d = 200$ ns). (a) Collected sub-pulses. (b) Reference signal. (c) Reconstructed baseband pulse.

parameters are altered, namely, the number of intra-pulses (N) and the amount of artificial delay (t_d) inserted into the setup. The variation of these parameters are as summarized in Table 4. The collected intra-pulses are processed into a wide bandwidth signal and finally, the ACF function of the re-constructed signal is plotted.

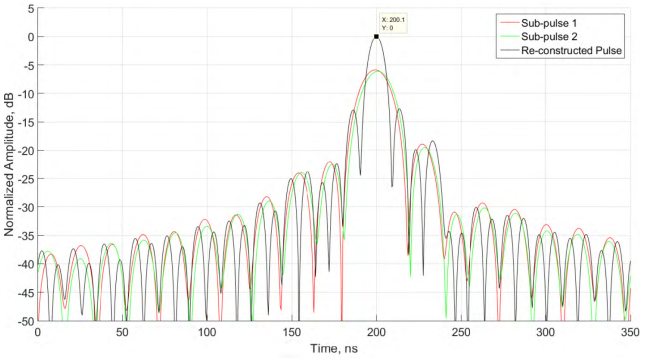

FIGURE 35. ACF of reconstructed baseband pulse ($N = 2$, $t_d = 200$ ns).

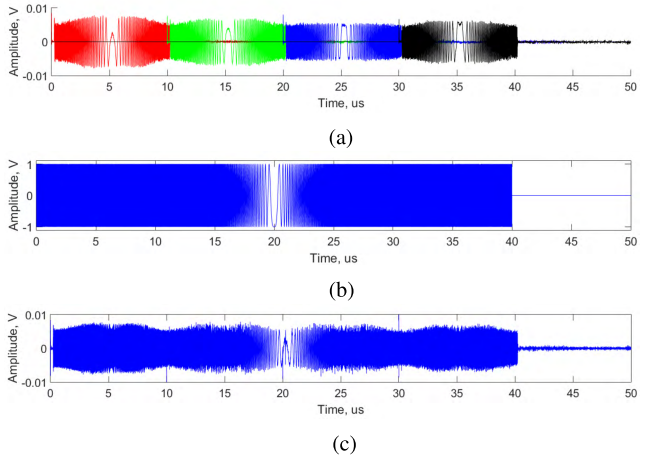

FIGURE 36. Recorded sub-pulses ($N = 4$, $t_d = 200$ ns). (a) Collected sub-pulses. (b) Reference signal. (c) Reconstructed baseband pulse.

TABLE 6. Advantages and disadvantages of the proposed phase coded SF_C-LFM.

Advantages	Disadvantages
• Greater bandwidth with minimal system hardware re-design • Wider pulse width with minimal system hardware re-design • Wider bandwidth whilst maintaining the system range (for ambiguity low altitude SAR scanning • Better SNR (due to increase in PCR) • Lower data transfer rate required as compared to its equivalent bandwidth system • Additional phase coding scheme introduces encryption in SAR system for data security	• More complex RF transmitter • Additional intra-pulse reconstruction process is required • Greater amount of data to be recorded

Figure 28 - Figure 33 show the results of adding a 100 ns delay to the setup while Figure 34 - Figure 39 are the results of adding a 200 ns delay to the setup. Figure 28, Figure 30,

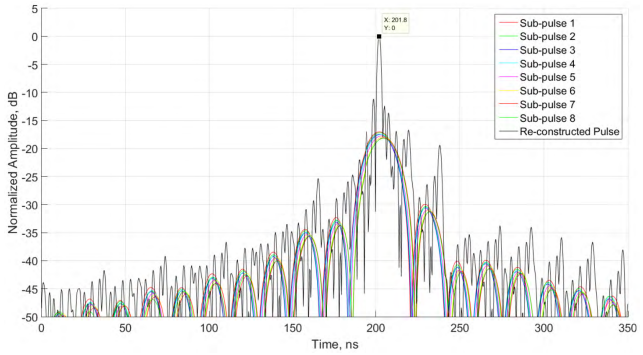

FIGURE 37. ACF of reconstructed baseband pulse ($N = 4$, $t_d = 200$ ns).

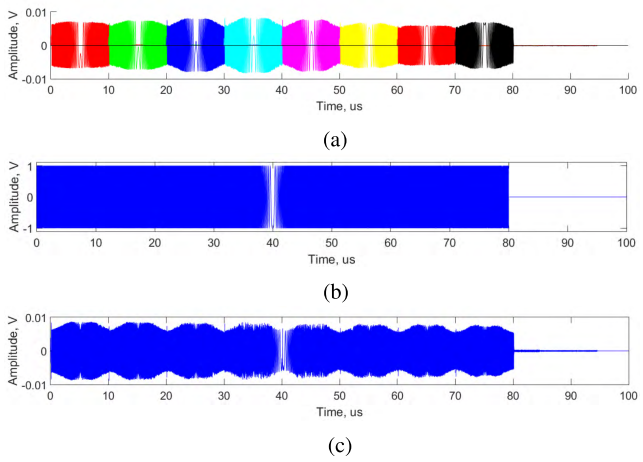

FIGURE 38. Recorded sub-pulses ($N = 8$, $t_d = 200$ ns). (a) Collected sub-pulses. (b) Reference signal. (c) Reconstructed baseband pulse.

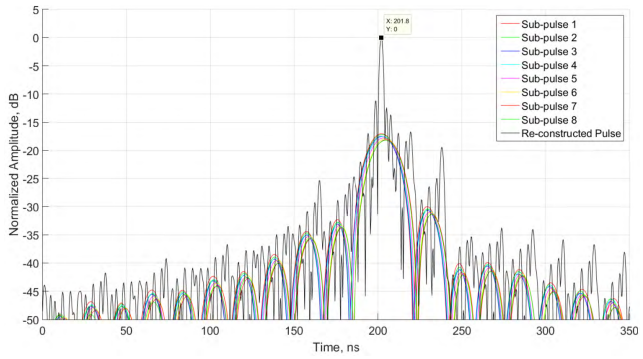

FIGURE 39. ACF of reconstructed baseband pulse ($N = 8$, $t_d = 200$ ns).

Figure 32, Figure 34, Figure 36, and Figure 38 compare the recorded intra-pulses with its combined pulse in time domain. Figure 29, Figure 31, and Figure 33 show a significant return with a 100 ns delay after range compression, while Figure 35, Figure 37, and Figure 39, show a significant return with a 200 ns delay after range compression. On the other hand, the measured Peak Side-Lobe Ratio (PSLR) and the improvement in Impulse Response Width (IRW) obtained for the SF_c-LFM system is summarized in Table 5. Table 6 summarizes the advantages and disadvantages of the proposed phase coded SF_c-LFM SAR scheme.

VI. CONCLUSION

In conclusion, a reconfigurable UWB SAR signal synthesis technique using the phase coded SF_c-LFM modulation scheme has been proposed. The proposed technique can synthesize a wider bandwidth and a wider pulse width signal compared to a conventional SAR system. As a result, this improves the SNR of a SAR system by improving the PCR of its transmitting waveform. Additionally, the phase coding scheme enhances the immunity of the radar system particularly on the electronics countermeasure of the radar system [16].

In summary, Section IV outlines the implementation and validation of the proposed technique. The results presented in Section V conclude that SF_c-LFM technique is able to improve the range resolution of the SAR system whilst maintaining its signal quality. The most significant advantage of the proposed technique is that it can improve the range resolution of an existing SAR system with minimal hardware re-design.

REFERENCES

[1] M. I. Skolnik, *Radar Handbook*. New York, NY, USA: McGraw-Hill, 1970.
[2] F. T. Ulaby, R. K. Moore, and A. K. Fung, *Microwave Remote Sensing: Active and Passive*. Norwood, MA, USA: Artech House, 1981.
[3] Y. K. Chan and S. Y. Lim, "Synthetic aperture radar (SAR) signal generation," *Progr. Electromagn. Res. B*, vol. 1, no. PIERB 01, pp. 269–290, 2008.
[4] E. Levanon and E. Mozeson, *Radar Signals*, 1st ed. Hoboken, NJ, USA: Wiley, 2004.
[5] B. Li, B. Zhang, Y. Fei, and Z. Qi, "A design of high-range resolution radar signal synthesizer," in *Proc. 3rd IEEE Int. Symp. Microw., Antenna, Propag. EMC Technol. Wireless Commun.*, Oct. 2009, pp. 74–77.
[6] N. J. Marechal, S. S. Osofsky, and R. M. Bloom, "Demonstration of W-band SAR imagery with a ground based system having 7.5 GHz of bandwidth obtained with a stepped chirp waveform," *IEEE Trans. Aerosp. Electron. Syst.*, vol. 49, no. 4, pp. 2522–2532, Oct. 2013.
[7] S. Matsuo, T. Fujimura, I. Oihara, E. Totsuka, Y. Ohura, and T. Kimura, "The digital wide band chirp pulse generator and processor for Pi-SAR2," in *Proc. IEEE Int. Geosci. Remote Sens. Symp.*, Jul. 2010, pp. 2872–2875.
[8] N. Salerno, L. Simone, S. Cocchi, V. Piloni, M. Maffei, and O. Cocciolillo, "Wideband arbitrary waveform generator for enhanced spaceborne SAR," in *Proc. Eur. Radar Conf.*, Oct. 2008, pp. 416–419.
[9] M. Sheng, H. Liu, J. Wang, and H. Jiang, "Direct digital generation of ultra-wideband lfm signal and its compensation technology," in *Proc. IET Int. Radar Conf.*, 2013, pp. 1–4.
[10] J. C. Curlander and R. N. McDounough, *Synthetic Aperture Radar, Systems and Signal Processing*, 1st ed. Norwood, MA, USA: Wiley, 1991.
[11] D. K. Barton, *Modern Radar System Analysis*, 1st ed. Norwood, MA, USA: Artech House, 1988.
[12] D. R. Wehner, *High Resolution Radar*, 2nd ed. Norwood, MA, USA: Artech House, 1987.
[13] Y. Mao, "FMCW radar receiver front-end design," Ph.D. dissertation, Dept. Elect. Eng., Math. Comput. Sci., Microelectron., Delft Univ. Technol., Delft, The Netherlands, 2009.
[14] M. Y. Chua and V. C. Koo, "FPGA-based chirp generator for high resolution UAV SAR," *Prog. Electromagn. Res.*, vol. 99, no. PIER 99, pp. 71–88, 2009.
[15] M. Y. Chua *et al.*, "A miniature real-time re-configurable radar waveform synthesizer for UAV based radar," *Prog. Electromagn. Res. C*, vol. 31, no. PIERC 31, pp. 169–183, 2012.
[16] M. Soumekh, "SAR-ECCM using phase-perturbed LFM chirp signals and DRFM repeat jammer penalization," *IEEE Trans. Aerosp. Electron. Syst.*, vol. 42, no. 1, pp. 191–205, Jan. 2006.

MING YAM CHUA was born in Malacca, Malaysia, in 1980. He received the B.Eng. degree (Hons.) in electronics from Multimedia University, Malaysia, in 2003, and the M.Eng.Sc. and Ph.D. degrees in engineering, with a focus on passive microwave components design and radar waveform synthesis techniques, from Multimedia University in 2007 and 2016, respectively.

He was with Multimedia University as a Researcher from 2003 to 2009, a Lecturer from 2009 to 2012, and a Senior Lecturer from 2012 to 2016. He is currently an Assistant Professor with the Center for Environmental Remote Sensing, Chiba University, Japan, undergoing his two years postdoctoral research leave from Multimedia University. His research interests are in the areas of synthetic aperture radar system development, with emphasis on radar waveform synthesis and field programmable gate array applications on radar systems.

VOON CHET KOO received the B.Eng. degree (Hons.) in electrical engineering from the University of Malaysia in 1997, and the M.Eng.Sc. and Ph.D. degrees in electrical engineering from Multimedia University, Malaysia, in 1999 and 2005, respectively. He is currently a Professor and the Chairperson of the Centre of Remote Sensing and Surveillance Technologies, Multimedia University. He received the inaugural Young Engineer Award by the Institution of Engineers, Malaysia, in 2004. He is also the Chairperson of the IEEE Malaysia Section Geoscience and the Remote Sensing Society Chapter, and a Fellow of the ASEAN Academy of Engineering and Technology.

HENG SIONG LIM received the B.Eng. degree (Hons.) in electrical engineering from Universiti Teknologi Malaysia in 1999, and the M.Eng.Sc. and Ph.D. degrees in engineering, with a focus on signal processing for wireless communications, from Multimedia University in 2002 and 2008, respectively. He is currently an Associate Professor with the Faculty of Engineering and Technology, Multimedia University. His current research interests are in the areas of signal processing for advanced wireless communications, with emphasis on detection and estimation theory and their applications.

JOSAPHAT TETUKO SRI SUMANTYO (S'00–A'02–M'04–SM'12) was born in Bandung, Indonesia, in 1970. He received the B.Eng. and M.Eng. degrees in electrical and computer engineering (subsurface radar systems) from Kanazawa University, Japan, in 1995 and 1997, respectively, and the Ph.D. degree in artificial system sciences (applied radio wave and radar systems) from Chiba University, Japan, in 2002.

From 2002 to 2005, he was a Lecturer (Postdoctoral Fellowship Researcher) with the Center for Frontier Electronics and Photonics, Venture Business Laboratory, Chiba University, Japan. From 2005 to 2013, he was an Associate Professor (permanent staff) with the Center for Environmental Remote Sensing, Chiba University, where he is currently a Full Professor (permanent staff). His research interests are theoretically scattering microwave analysis and its applications in microwave (radar) remote sensing, especially synthetic aperture radar and subsurface radar (VLF), including DInSAR and PS-InSAR, analysis and design of antennas for mobile satellite communications and microwave sensors, development of microwave sensors, including SAR for unmanned aerial vehicle and microsatellite development.